Frequency Response Mechanisms for the GaAs MSM Photodetector and Electron Detector

Tamera A. Yost, Asher Madjar, *Fellow, IEEE,* and Peter R. Herczfeld, *Fellow, IEEE*

***Abstract*—The GaAs metal–semiconductor–metal (MSM) device is a very useful planar and monolithic-microwave integrated-circuit compatible photodetector and electron-detector. As a photodetector, the MSM has been used for many applications in the past, however, in this paper we demonstrate its usefulness as an electron-beam detector as well. We present here a comprehensive analysis of the primary detection mechanism (electric field enhanced collection of generated electrons) as well as a newly identified secondary mechanism. This new mechanism is characterized by a high detection gain, but low speed. Experimental results are presented to verify the analysis, and possible applications are suggested by utilizing each one of the two detection mechanisms.**

***Index Terms*—Electron detector, GaAs, MSM device, photo detector, photo tubes.**

I. INTRODUCTION

The GaAs metal–semiconductor–metal (MSM) device is a planar device composed of two back-to-back Schottky junctions. It is usually constructed as an array of interdigital metal electrodes deposited on top of a GaAs undoped epitaxial layer grown on a semiinsulating GaAs substrate. The details of the MSM structure are presented in Section II. The device is usually operated by applying dc bias of a few volts across its terminals, thus establishing an electric field, which is well above the threshold for electron velocity saturation. When used as a photodetector, the device is illuminated from the top by an intensity modulated light beam. The photons are absorbed by the GaAs material and produce electron–hole pairs. These charge carriers induce electric current in the device, thus constituting the desired photodetection effect.

The same MSM device can be used also as an electron detector. This is achieved by bombarding the device with a beam of high-energy electrons. The electrons enter the GaAs material and cause impact ionization of the crystal molecules, thus creating a large number of free electrons, which induce electric current in the device. Since each electron can ionize a large number of molecules a gain mechanism is established. Such utilization of the MSM device can be realized in a large area phototube. Phototubes are used in free-space optical communications, inter-satellite communications and microwave modulated lidar–radar systems. The phototubes are vacuum tubes containing: a light sensitive photocathode (releases free electrons when illuminated), an electric field based focusing mechanism and an anode device, which is an electron-detector (preferably with gain). The use of the MSM device as an anode for the phototube has been demonstrated successfully by the authors [1].

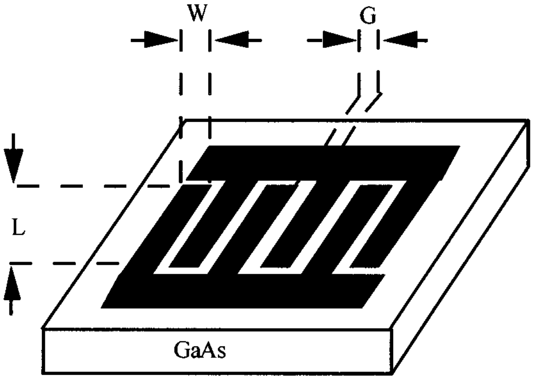

Fig. 1. Interdigital MSM device.

In this paper, we present an analysis of the MSM device, which is valid for both light or electron detection. The analysis considers the following two independent detection mechanisms: 1) the primary effect—electric field enhanced collection of charge carriers in the high electric field depletion region and 2) a secondary effect related to the interface between substrate and epitaxial-layer. The primary effect is relatively wideband (a few gigahertz), but low gain (optical responsivity <1). The secondary effect is narrow band (slow-megahertz range), but high gain and of a logarithmic nature. By suppressing one or the other effect one can get either a low responsivity fast detector or a high responsivity slow detector.

In Section II the structure of the MSM device is presented. The analysis of the device in the primary and secondary modes is presented in Sections III and IV, respectively. The theoretical analysis is verified by experimental results presented in Section V. Discussion of the results, possible applications and conclusions are presented in Sections VI and VII.

II. MSM DEVICE STRUCTURE

The MSM is constructed by placing contacts of a specific material in a lateral configuration on semiconductor substrates. The physical nature of the contact-semiconductor junction could be rectifying or ohmic, identifying the device as a photodiode or a photoconductor, respectively. The geometry of an interdigital MSM is shown in Fig. 1 and consists of metal pads and electrodes deposited on bulk GaAs.

The electrodes have a length L, width W, and gap spacing G. Essentially, the device is two Schottky diodes in a back-to-back arrangement, since one electrode has a positive bias and the other a negative bias. In this bias arrangement, one contact is

Manuscript received November 6, 2000; revised June 21, 2001.

The authors are with the Center for Microwave-Lightwave Engineering, Electrical and Computer Engineering Department, Drexel University, Philadelphia, PA 19104 USA.

Publisher Item Identifier S 0018-9480(01)08711-7.

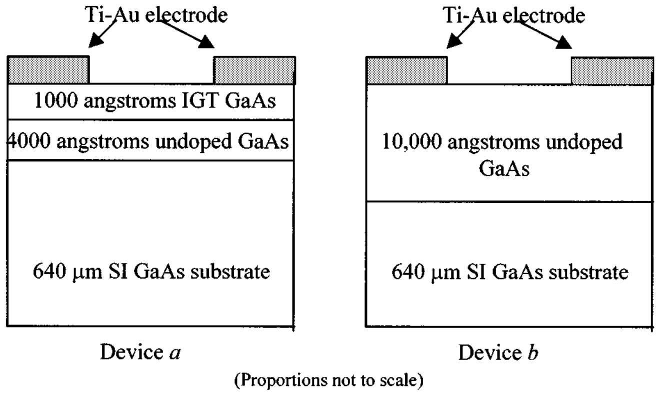

Fig. 2. Cross-sectional view of MSM (Device *a*: "thin channel" and Device *b*: "thick channel").

forward biased and the other reverse biased, leading to reduced dark current compared to a photoconductive detector. The dopant density of the semiconductor is usually low to achieve full depletion of majority carriers in the region between the contacts. When used as a photodetector, incident photons with energy larger than the bandgap of the semiconductor strike the region of bare semiconductor and are absorbed, resulting in the upward transition of a free electron from the valence band to the conduction band. The MSM as an electron bombarded semiconductor device is a novel application. There are some significant differences between the operation of the MSM as a photodetector versus that of an electron detector. First, incident high energy electrons will not be masked by the electrodes, but penetrate the metal and contribute to the overall device gain. Second, the carrier generation process is not due to absorption, but to impact ionization of the semiconductor material. The incident electron creates an electron–hole pair by an inelastic collision with an atom, breaking the covalent bond to free an electron, and giving sufficient energy to the free electron to transition from the valence band to the conduction band. Large current gains are typical because each electron in the beam creates more than a thousand electron–hole pairs in the semiconductor. Gain occurs as the incident energetic electrons excite valence band electrons to the conduction band as they penetrate the semiconductor. The amount of gain is proportional to the amount of energy of the incident electron and the energy needed to generate the electron–hole pair. The electrons in the conduction band and the holes in the valence band travel in opposite directions by the field in the depletion region, which is enhanced by an applied field. The transit of the charges constitutes a current and the recombination of an electron–hole pair at a contact signals the measurement of a photon or electron beam induced carrier. It is important to note that an MSM device can be used as an electron detector for radiation levels below the damage level to the crystal, which depends on the specific material structure.

In this paper, we analyze and present experimental results for the two MSM structures shown in Fig. 2. Device a represents the high gain slow detector, while Device *b* represents the low gain high speed detector. The wafer structure of Device *a* consists of a 1000 Å layer of Intermediate Growth Temperature (IGT-350 °C) GaAs grown on 4000 Å of an undoped GaAs buffer layer and Device *b* consists of a 10 000-Å layer of undoped GaAs. Device *a* is described as a "thin channel" device since the total active GaAs layer is only 5000 Å or 0.5 μm, while the "thick channel" device has an active layer thickness of 10 000 Å or 1 μm. Both wafers were grown using molecular-beam-epitaxy (MBE) methods from a commercial wafer supplier.

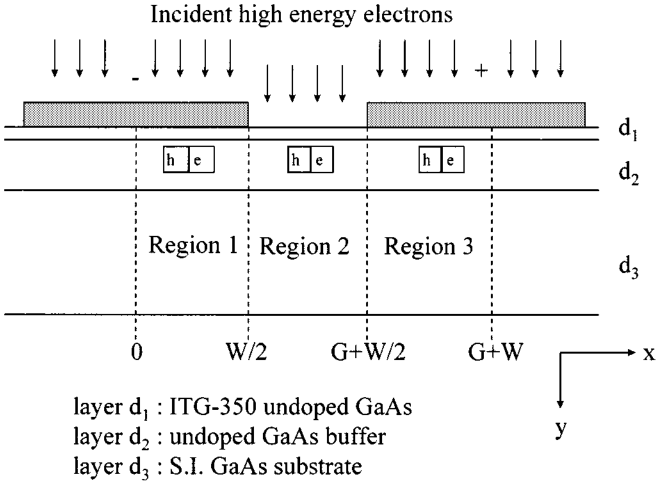

Fig. 3. Electron bombarded MSM physical layout.

III. THE PRIMARY DETECTION MECHANISM

Various approaches have been taken in modeling the frequency and time response of MSM devices under optical excitation, including Monte Carlo techniques, linear state-space analysis, and correlation methods. This paper does not concern the evaluation or development of the dynamic response of MSM photodetectors. Therefore, theoretical analysis of the primary photodetection process is performed using a simplified one-dimensional (1-D) analytical transit-time limited model previously published [2]. A novel theoretical analysis of the primary electron detection process is, however, presented here.

In developing an accurate frequency response model of the primary detection mechanism for electron detection, special interest was paid to the transit time of carriers generated in the different regions and layers of the active semiconductor material for the "narrow" channel device shown in Fig. 3. The device consists of three semiconductor layers of thickness d_1, d_2, and d_3. The two active layers are d_1 and d_2, which are undoped intermediate temperature grown (IGT-350 °C) GaAs and an undoped GaAs buffer, respectively. The third layer is a semiinsulating (SI) GaAs substrate. For our samples the total thickness of the two active layers is much less than the gap between electrodes or the electrode width.

The two layers of active semiconductor have very different parameters that will effect the collection of the generated electron–hole pairs. The layer of IGT GaAs was chosen to reduce the device dark current.

A two-dimensional (2-D) model was developed that determines the transit-time limited frequency response of the MSM for single or multiple active layer devices in detail in [6] with a summary presented in this paper. However, the devices of interest are not strictly transit-time limited and the device capacitance must be accounted for. This is accomplished by using the transit-time limited current response from the model as a frequency dependent current source in the equivalent *RC* circuit of the MSM. The model assumes an applied bias large enough to saturate both electrons and holes, such as 15 V. Thereby, the carriers that are collected at the electrode are assumed to travel their effective transit length at saturation velocity. Diffusion current is neglected and current flow is accounted for in the x direction only.

Referring to Fig. 3, the average distance an electron or hole must travel before being collected at the electrode depends in which region it was generated. In region 1 under the negative electrode, a hole will be collected quickly since it has only to travel from the creation point to the electrode. The length an electron must travel is from the creation point plus the distance between electrodes to reach the positive electrode. In region 2, both holes and electrons must travel from the creation point to the respective electrode. In region 3, the same transit distances occur as in region 1, but for opposite carriers. An approximation to their effective transit length is assumed where the average distance is the semi-circumference of an ellipse with appropriate radii for that region.

The development of the transit-time limited frequency response begins with the solution of the continuity equation. The continuity equations for electrons and holes, respectively, are

$$\frac{\partial n}{\partial t} = \frac{1}{q}\nabla\cdot J_n + G - R$$

$$\frac{\partial p}{\partial t} = -\frac{1}{q}\nabla\cdot J_p + G - R \tag{1}$$

where

$$J_n = qnv_n \tag{2}$$

$$J_p = qpv_p. \tag{3}$$

The continuity equations are solved in each region and layer to account for the different generation rates of each region and semiconductor parameters of each layer. The current density from each area contributes to the total current. Since the generation rate varies sinusoidally, the device current will also. Therefore, the current density will be of the form $J_n e^{j\omega t}$ and $J_p e^{j\omega t}$ in the continuity equations.

The carrier generation rate for a incident beam of energetic electrons can be expressed as

$$G_{eb}(y) = \frac{J_B}{q\varepsilon_p}\frac{fE_i}{R}\left(0.60 + 6.21\frac{y}{R} - 12.40\left(\frac{y}{R}\right)^2 + 5.69\left(\frac{y}{R}\right)^3\right) \tag{4}$$

where J_B is the electron beam current density, f is the electron backscatter, E_i is the incident electron beam energy, ε_p is the average energy required to produce ionization, and R is the stopping distance of the incident electron in the GaAs [8]. Given the generation rate in (4) is y-dependent, a per-unit-length ac electron current ($J_n\Delta y$) flows in a layer of thickness Δy. The solution of the continuity equation is presented for electrons and holes in the six regions. It is important to note that this approach of separate treatment of electron and hole currents is valid for practical levels of light or electron illumination. Obviously for very high levels of radiation space charge may be formed, which causes interaction between holes and electrons.

A. Electron Current Density

The electron current density for the IGT GaAs layer in region 1 under the electrode is

$$J_{n1a}(j\omega) = \frac{qG_{1a}}{P_{n1a}}\left[\frac{1-\exp(P_{n1a}W/2)}{P_{n1a}W/2} + 1\right] \tag{5}$$

and in the undoped GaAs layer is

$$J_{n1b}(j\omega) = \frac{qG_{1b}}{P_{n1b}}\left[\frac{1-\exp(P_{n1b}W/2)}{P_{n1b}W/2} + 1\right]. \tag{6}$$

The electron current density for the IGT GaAs layer between the electrodes is

$$J_{n2a}(j\omega) = \frac{qG_{2a}}{P_{n2a}} + \frac{1}{P_{n2a}G}\left[J_{n1a}(W/2) - \frac{qG_{2a}}{P_{n2a}}\right]\cdot[\exp(P_{n2a}G) - 1] \tag{7}$$

and in the undoped GaAs layer is

$$J_{n2b}(j\omega) = \frac{qG_{2b}}{P_{n2b}} + \frac{1}{P_{n2b}G}\left[J_{n1b}(W/2) - \frac{qG_{2b}}{P_{n2b}}\right]\cdot[\exp(P_{n2b}G) - 1]. \tag{8}$$

The electron current density for the IGT GaAs layer in region 3 under the electrode is

$$J_{n3a}(j\omega) = \frac{qG_{1a}}{P_{n3a}} + \frac{1}{P_{n3a}W/2}\left[J_{n2a}(W/2+G) - \frac{qG_{1a}}{P_{n3a}}\right]\cdot[\exp(P_{n3a}W/2) - 1] \tag{9}$$

and in the undoped GaAs layer is

$$J_{n3b}(j\omega) = \frac{qG_{1b}}{P_{n3b}} + \frac{1}{P_{n3b}W/2}\left[J_{n2b}(W/2+G) - \frac{qG_{1b}}{P_{n3b}}\right]\cdot[\exp(P_{n3b}W/2) - 1] \tag{10}$$

where $G_{\#x}$ represents the generation rate for that region, $P_{n\#x}$ for each region is

$$P_n = \left(\frac{1}{\tau_n} + j\omega\right)\Big/ v_n = \frac{1}{L_e}\left(\frac{\tau_{tr}}{\tau_n} + j\omega\tau_{tr}\right)$$

where τ_n and τ_{tr} are the electron recombination lifetime and transit times, v_n is the electron drift velocity, L_e is the effective transit distance, and W and G are the electrode width and gap dimensions. A similar set of equations for hole current density are presented below.

B. Hole Current Density

In solving the continuity equation for holes, the known boundary condition is that $J_p(W+G)\Delta y = 0$ or the current has to equal zero at the positive electrode. In solving for the current density of electrons, the boundary conditions were satisfied at $x = 0$, $W/2$, and $W/2+G$. In solving the continuity equations for holes, the boundary conditions are satisfied at $x = W/2$, $W/2+G$, and $W+G$. The approach to the solution for hole current density is the same as for electron current density, except for boundary conditions. The result for all regions and layers is summarized below since the derivation is similar to electrons.

In region 1, the hole current density expressions for each layer are

$$J_{p1a}(j\omega) = \frac{qG_{1a}}{P_{p1a}} + \frac{1}{P_{p1a}W/2}\left[J_{p2a}(W/2) - \frac{qG_{1a}}{P_{p1a}}\right] \cdot [\exp(P_{p1a}W/2) - 1] \tag{11}$$

$$J_{p1b}(j\omega) = \frac{qG_{1b}}{P_{p1b}} + \frac{1}{P_{p1b}W/2}\left[J_{p2b}(W/2) - \frac{qG_{1b}}{P_{p1b}}\right] \cdot [\exp(P_{p1b}W/2) - 1]. \tag{12}$$

In region 2, the hole current density expressions for each layer are

$$J_{p2a}(j\omega) = \frac{qG_{2a}}{P_{p2a}} + \frac{1}{P_{p2a}G}\left[J_{p3a}(W/2+G) - \frac{qG_{2a}}{P_{p2a}}\right] \cdot [\exp(P_{p2a}G) - 1] \tag{13}$$

$$J_{p2b}(j\omega) = \frac{qG_{2b}}{P_{p2b}} + \frac{1}{P_{p2b}G}\left[J_{p3b}(W/2+G) - \frac{qG_{2b}}{P_{p2b}}\right] \cdot [\exp(P_{p2b}G) - 1]. \tag{14}$$

In region 3, the hole current density expressions for each layer are

$$J_{p3a}(j\omega) = \frac{qG_{1a}}{P_{p3a}}\left[\frac{1 - \exp(P_{p3a}W/2)}{P_{p3a}W/2} + 1\right] \tag{15}$$

$$J_{p3b}(j\omega) = \frac{qG_{1b}}{P_{p3b}}\left[\frac{1 - \exp(P_{p3b}W/2)}{P_{p3b}W/2} + 1\right]. \tag{16}$$

As with the electron formulation, $G_{\#x}$ represents the generation rate for that region, $P_{n\#x}$ for each region is

$$P_p = \left(\frac{1}{\tau_p} + j\omega\right)\Big/ v_p = \frac{1}{L_e}\left(\frac{\tau_{tr}}{\tau_p} + j\omega\tau_{tr}\right)$$

where τ_p and τ_{tr} are the hole recombination lifetime and transit times, v_p is the electron drift velocity, L_e is the effective transit distance, and W and G are the electrode width and gap dimensions.

C. Total Current Density

The total frequency dependent current density is the summation of all individual components

$$J_n(j\omega) = J_{n1a}(j\omega) + J_{n1b}(j\omega) + J_{n2a}(j\omega) + J_{n2b}(j\omega) + J_{n3a}(j\omega) + J_{n3b}(j\omega) \tag{17}$$

$$J_p(j\omega) = J_{p1a}(j\omega) + J_{p1b}(j\omega) + J_{p2a}(j\omega) + J_{p2b}(j\omega) + J_{p3a}(j\omega) + J_{p3b}(j\omega) \tag{18}$$

$$J(j\omega) = J_n(j\omega) + J_p(j\omega). \tag{19}$$

The previous section dealt with the solution of the continuity equation for electrons and holes in all six regions of the MSM. The average current densities were found by integrating over the physical dimensions and the total average current density is found by combining the responses of the individual components. The total current density $J(j\omega)$ is used as the frequency dependent current source for the MSM equivalent circuit.

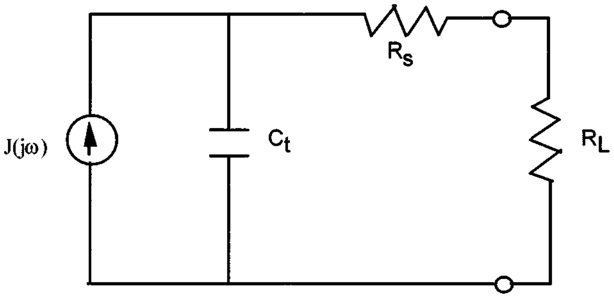

Fig. 4. Simplified MSM equivalent circuit.

Using the frequency dependent current response derived from the transit-time limited model and the transfer function of the equivalent circuit of Fig. 4, the complete frequency response of the MSM including capacitance and transit-time effects can be represented by

$$J_o(j\omega) = \frac{1}{1 + j\omega C_t(R_s + R_L)}\, J(j\omega) \tag{20}$$

where $J(j\omega)$ is defined in (19).

IV. The Substrate-Epitaxial Layer Barrier Related Detection Process

In this section we present an analysis of a secondary detection mechanism related to the interface between the semiinsulating substrate and the epitaxial layer. This effect is very similar to an effect identified and analyzed by part of the authors for the MESFET as an optical detector [4]–[8]. For the MESFET we termed this the "internal" photovoltaic effect. For the MSM device this may be termed the internal unintentional bipolar transistor effect.

The difference in the background doping level between the epitaxial layer and the semiinsulating substrate and subsequent diffusion of electrons from the epitaxial layer to the substrate gives rise to a potential barrier

$$V_{\text{bar}} = \eta_b (kT/q) \ln(n_e/n_s). \tag{21}$$

On the epitaxial side, the space charge is created by the positively charged ionized donors, left behind by the migrating electrons. In this region the space charge density is qn_e and its height is denoted by Δ. On the substrate side, a negative charge distribution is established due to the electrons which have diffused from the epitaxial layer. These electrons tend to concentrate close to the physical barrier, adjacent to the ionized donors. Therefore, it is assumed that the charge distribution is a delta function at the barrier. Following the analysis in [4], the expression for the potential barrier is

$$V_{\text{bar}} = qn_e\Delta^2/(2\varepsilon). \tag{22}$$

Alternatively, we can solve for Δ

$$\Delta = [2\varepsilon V_{\text{bar}}/(qn_e)]^{1/2} \tag{23}$$

$\varepsilon = \varepsilon_0\varepsilon_r$ is the dielectric permitivity of GaAs. Thus, for given doping densities the barrier potential can be calculated from (21) and the barrier height is calculated from (23). The above expressions are valid for the "dark" status, namely, no type of excitation is applied to the device (except dc). When the MSM device is either illuminated by light or bombarded by electron flux, generation of electron–hole pairs takes place in the device volume (the penetration depth of both light and electrons depends on light wavelength and electron beam energy level, however, a typical value is around 1 μm for GaAs). If the epitaxial layer thickness is substantially bigger than the penetration depth there is no generation of electon-hole pairs in the barrier region, and the only detection mechanism is the primary effect presented in Section III. This applies to some degree to device type b (thick channel) in Fig. 2. On the other hand, for epitaxial layers thin compared to the penetration depth, electron–hole pair generation occurs in the barrier region (in addition to the bulk of the device). In this case, in addition to the primary detection mechanism, there exists another phenomenon, which increases substantially the current via the device. This can be explained as follows: The barrier region is a high field region due to the built-in electric field, so the electron–hole pairs generated by the exciting signal (light or electron flux) establish a current between the epitaxial layer and the substrate (the electrons flow into the epitaxial layer and the holes flow into the substrate). This current is in fact the base current of a "parasitic" bipolar transistor. The MSM anode finger acts as the collector, the cathode finger acts as the emitter and the substrate adjacent to the barrier acts as the base. This "transistor" has no base contact, so that current cannot be applied to it electronically, however, the illumination generates the base current for the transistor. This base current is amplified by the transistor and manifests itself as a "collector" current contributing directly to the MSM device current. Due to the amplifying effect of the transistor, this "parasitic" effect may in fact be stronger than the primary effect, as shown by measurements in Section V. On the other hand, this parasitic transistor has a long base, so that it is very slow, and therefore this secondary effect is much slower compared to the primary effect (megahertz operation versus gigahertz operation).

We denote the MSM current due to this effect by I_{sub}, since it is the current contribution due to conduction via the substrate. This current can be expressed as

$$I_{\text{sub}} = \beta I_{\text{base}} \tag{24}$$

where β is the common emitter current gain of the "bipolar transistor" (Sze [9]) and I_{base} is the effective base current

$$\beta = 1/[\cosh(W_B/L_n) - 1]. \tag{25}$$

The effective "base width " W_B is estimated as the average distance of travel for the electrons from "collector" to "emitter" in the substrate. For light illumination $W_B = G$ (gapwidth). For electron illumination the effective base width is somewhat bigger, but the same value can be used as a reasonable estimate. The base current expression can be derived by calculating the total current via the barrier due to the excitation. For light illumination, the calculation follows the one presented in [4]. The result is

$$I_{\text{base}} = 2qGL(n-1)F_{ph}\exp(-\alpha(a_e+\Delta_i))\alpha\Delta_i \tag{26}$$

where, for G, L, see Fig. 1, n is the number of fingers, $F_{ph} = T_r P_{opt}/h\nu = T_r \lambda P_{opt}/hc$ is the absorbed photon flux per unit area per unit time, α is the light absorption coefficient, $a_e = d_1 + d_2$ is the epitaxial layer height, and Δ_i is the barrier height **under illumination** (see derivation below). For the electron bombardment case, the calculation is based on the generated electron and hole density expression derived in Section III [(3)-(4)]. The above density expression needs to be integrated over the barrier region $(y = a_e$ to $y = a_e + \Delta_i)$ to calculate the total amount of electrons, N (and holes P) collected in the barrier per unit time per unit area. The result is

$$N = P = (J_B f E_i)/(q\varepsilon_p R)F(a_e,\, \Delta_i) \tag{27}$$

where

$$\begin{aligned} F(a_e,\, \Delta_i) = {}& 0.6\Delta_i + (3.105/R)\Big[(a_e+\Delta_i)^2 - a_e^2\Big] \\ & - (4.133/R^2)\Big[(a_e+\Delta_i)^3 - a_e^3\Big] \\ & + (1.4225/R^3)\Big[(a_e+\Delta_i)^4 - a_e^4\Big]. \end{aligned} \tag{28}$$

Assuming that all the electrons and holes are collected (due to the high electric field in the barrier region), the expression for the base current is

$$I_{\text{base}} = (2J_B f)/(\varepsilon_p R)[E_w(n-1)GL + E_m nWL]F(a_e,\, \Delta_i). \tag{29}$$

The variables are same as for (4) and Fig. 1, except E_w is the incident electron beam energy in the window regions and E_m is the incident electron beam energy in the metalized regions.

From (24) it is obvious that for a given device the detected current via the device is proportional to I_{base}. Looking at the expressions in (26) or (29) for I_{base}, one may conclude that the detection mechanism is linear since I_{base} seems to be proportional to the signal amplitude $(F_{ph}$ or $J_B)$. This conclusion however is incorrect, since the nonlinear dependence of I_{base} on the signal level enters via the barrier height Δ_i which is a function of the signal level. This can be demonstrated by deriving the equation for the barrier height under illumination. The current I_{base} via the barrier region under illumination is in fact lowering the barrier potential. Using the well known expression for the current in a diode the expression for the barrier voltage under illumination is

$$V_{\text{bari}} = \eta_b(kT/q)\ln(I_{\text{base}}/I_s + 1). \tag{30}$$

I_s is the reverse saturation current of the barrier diode, and can be expressed as

$$I_s = J_s[(n-1)G + nW]L \tag{31}$$

where J_s is the reverse saturation current density of the barrier diode. The relation between the barrier height and barrier potential is given in (22), and use of that equation in conjunction with (30), (31) produces the following nonlinear equation for the barrier height under illumination

$$\Delta_i^2 = 2\varepsilon\eta_b(kT/q^2 n_e)\ln[I_{\text{base}}/(J_s[(n-1)G + nW]L) + 1]. \tag{32}$$

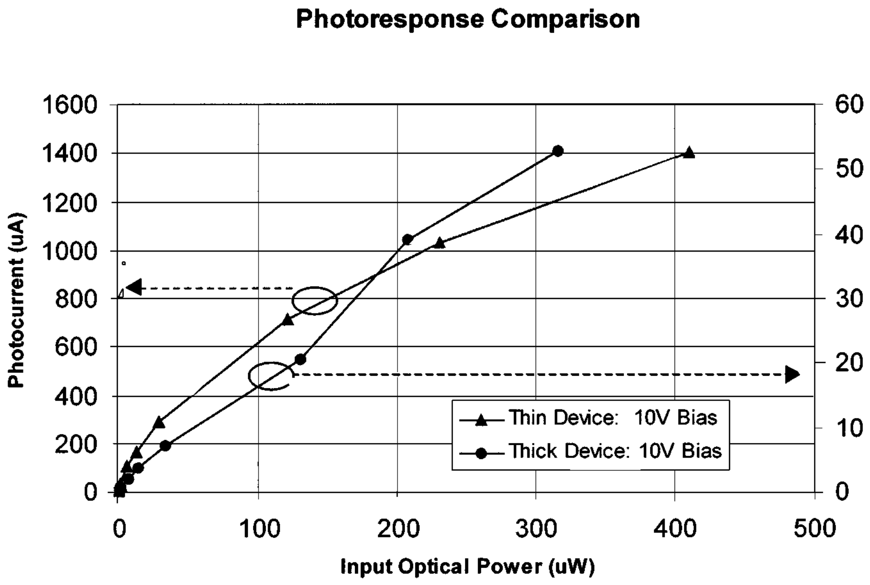

Fig. 5. Thin and thick device photoresponse versus optical power (thick-right scale, thin-left scale).

Depending on the excitation type, either (26) (light) or (29) (electrons) is used for I_{base} in (32). In either case this equation is solved numerically for Δ_i, the barrier height under illumination, using standard Newton–Raphson techniques. From (32) it is clear that the dependence of Δ_i on the signal level is of a logarithmic nature, thus the effect considered here is highly nonlinear and of a compressive nature.

The dynamic properties of this detection mechanism are dominated by the response time of the unintentional bipolar transistor. The charging and discharging of the barrier region is of course also a limiting factor to the speed of this effect, however, the transistor response is the most limiting one. It is known from basic transistor theory [9] that the transit time of the minority carriers via the base is expressed as

$$\tau_B = W_B^2/(2D_B) \tag{33}$$

where W_B is the base width and D_B is the diffusion coefficient of the minority charge carriers at the base. In our case the effective base width can be estimated at approximately the gapwidth G. Typically G is in the order of a few microns, while for a microwave transistor (cutoff frequency around 20 GHz) the base width is a few hundred angstrom ($\sim$500 A). Since the transit time is proportional to the square of the base width we can expect for our device ($G = 5$ μm) a cutoff frequency of about 2 MHz.

V. EXPERIMENTAL RESULTS

The theory and models presented in Sections III and IV were tested by a series of measurements. The results of these measurements are presented here. Due to practical constraints the measurements were performed with 850 nm light excitation only. The following two types of measurements were performed 1) constant illumination (unmodulated light) and 2) open-circuit photovoltage.

Fig. 5 depicts the photo currents of the MSM devices for a range of input optical power levels. The term “Thin device” refers to Fig. 2(a) and “Thick device” to Fig. 2(b). For both devices $W = 4$ μm, $G = 5$ μm and the active area is 300 μm × 300 μm. Note that the curve for the thin device relates to the left scale and for the thick device to the right scale. A very pronounced observation from Fig. 5 is the fact that the photo response of the **thin** device is more than an order of magnitude higher compared to that of the thick device. This fact clearly indicates that in addition to the primary effect (Section III) there exists some other effect, since for the primary effect the higher response is for the **thick** device, in contrast to the measurements. The explanation to this “contradiction” is that for the thick device the barrier is deep in the device, so that the secondary effect is small compared to the primary effect. In contrast, for the thin device the secondary effect is dominating the response, as expected from the model in Section IV. Another observation from Fig. 5 is that for the thick device the response is close to linear, which fits the primary effect model. In contrast, keeping in mind the different scales, for the thin device the response is of a compressive nature (logarithmic like), which indicates that the secondary effect is the dominant one for this device. More measurements of this type are depicted also in Fig. 6. However, in this figure we have used a log scale for both axes. Fig. 6 indicates clearly the logarithmic nature of the secondary effect in the thin device.

To demonstrate the existence of the secondary effect related to the epitaxial layer-substrate interface, we have measured the induced photo voltage across the MSM terminals when illuminated with an unmodulated light **without applying any dc voltage**. The results of this measurement are depicted in Fig. 7 for both devices. The results show an induced photo voltage, which is dependent on the optical power. As can be seen, for the thick device there is practically no photo voltage for low optical power levels. For high optical power levels, enough electron–hole pairs are generated in the barrier region to cause the secondary effect, and a photo voltage is created. For the thin device, photo voltage is observed even for low power level since the barrier region is not so deep and much more accessible to the light.

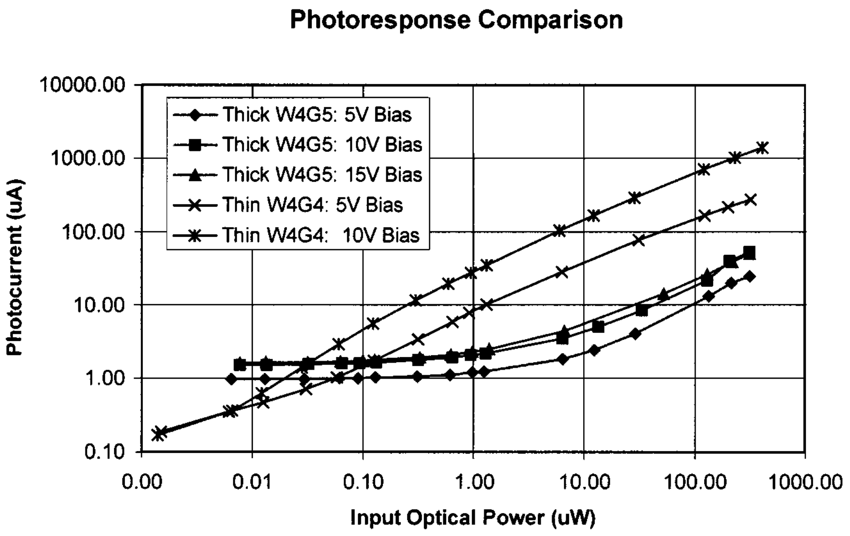

Fig. 6. Photoresponse comparison using log–log scale.

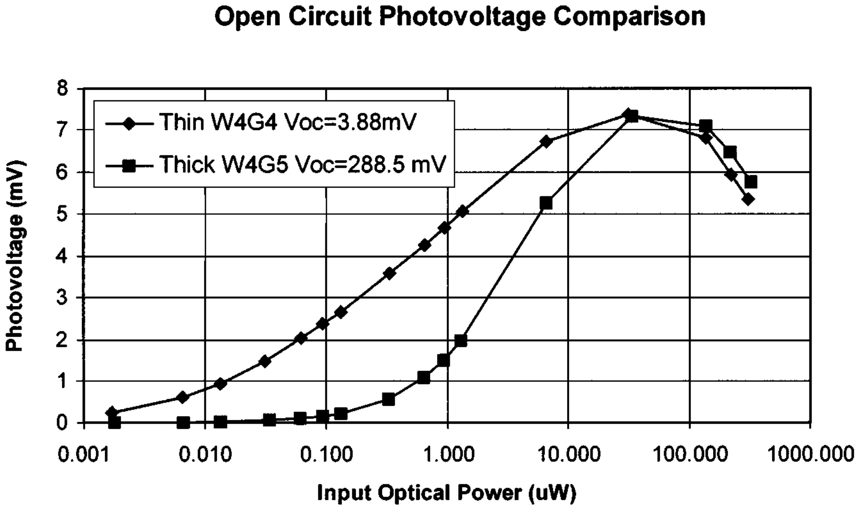

Fig. 7. Photovoltage comparison.

VI. DISCUSSION

The MSM device can be used as both a photo detector and an electron detector. We have identified two basic detection mechanisms: the primary effect related to the electric-field enhanced collection of the electron–hole pairs and the secondary effect related to the reduction of the barrier between the epitaxial layer and the substrate. The latter effect is causing current flow via the substrate. The primary effect is the “normal” expected response, which has been analyzed in the past for photodetectors, and analyzed here for the case of electron-detector. The secondary effect is a newly identified detection process in the MSM. The primary effect is basically linear, while the secondary effect is of a logarithmic nature. In addition, the primary effect is relatively fast, even for a large area detector (gigahertz range), while the secondary effect is very slow (megahertz range).

Due to the large difference between the two effects both in magnitude and speed, it seems that it would be undesirable to have both effects in the same device. Normally, one would like to enhance one of the effects and suppress the other. For applications requiring linear and fast detector it is desirable to enhance the primary effect (following the analysis in Section III) and suppressing the secondary effect. The suppression of the secondary effect can be done in a similar manner to the one used for suppressing substrate current in MMICs. The method is to insert a buffer layer between the substrate and the epitaxial layer during the process of growing the epitaxial layer. The buffer layer is made up of a large number of quantum wells. This can be achieved for example by MBE or MOCVD growth of monolayers of alternating GaAs and AlGaAs. Such a buffer layer prevents substrate current, since the charge carriers attempting to flow between substrate and epitaxial layer are trapped in the quantum wells.

For applications requiring a response of a compressive nature, such as a logarithmic response it is possible to enhance the secondary effect and suppress the primary effect. This can be achieved by reducing the height of the epitaxial layer. This causes both reduction of the primary effect (by decreasing the volume of the carrier collection) and increase of the secondary effect (by decreasing the distance between the barrier and the surface). One should keep in mind however that the secondary effect is very slow. Some improvement can be achieved in speed by reducing the gap size G. This causes a reduction in the transit time via the "base" and, thus, increases the cutoff frequency.

VII. CONCLUSION

A comprehensive model for the MSM device as a photo detector and electron-beam detector is presented in this paper. The modeling and analysis take into account both the primary detection mechanism based on electric field enhanced electron–hole collection and a newly identified secondary effect based on substrate conduction due to barrier lowering between the substrate and epitaxial layer. The analysis is supported by experimental results performed on two types of devices. Possible applications for the MSM device are suggested and design criteria are recommended.

REFERENCES

[1] T. A. Yost, "Large area, high speed phototube employing a metal–semiconductor–metal anode," Ph.D. dissertation, ECE Dept., Drexel Univ., Philadelphia, PA, June 1998.

[2] J.-W. Chen, D.-K. Kim, and M. B. Das, "Transit-time limited high-frequency response characteristics of MSM photodetectors," *IEEE Trans. Electron Devices*, vol. 43, pp. 1838–1843, Nov. 1996.

[3] T. E. Everhart and P. H. Hoff, "Determination of kilovolt electron energy vs penetration distance in solid materials," *J. Appl. Phys.*, vol. 42, no. 13, pp. 5837–5846, Dec. 1971.

[4] A. Madjar, P. R. Herczfeld, and A. Paolella, "Analytical model for optically generated currents in GaAs MESFETs," *IEEE Trans. Microwave Theory Tech.*, vol. 40, pp. 1681–1691, Aug. 1992.

[5] A. Paolella, A. Madjar, and P. R. Herczfeld, "Modeling the GaAs MESFET's response to modulated light at radio and microwave frequencies," *IEEE Trans. Microwave Theory Tech.*, vol. 42, pp. 1122–1130, July 1994.

[6] A. Madjar, A. Paolella, and P. R. Herczfeld, "Modeling the optical switching of MESFET's considering the external and internal photovoltaic effects," *IEEE Trans. Microwave Theory Tech.*, vol. 42, pp. 62–67, Jan. 1994.

[7] A. Madjar, A. Paolella, and P. R. Herczfeld, "The compressive nature of optical detection in GaAs MESFET's and possible applications as an RF logarithmic amplifier," *IEEE Trans. Microwave Theory Tech.*, vol. MTT-41, pp. 165–167, January 1993.

[8] A. Madjar and P. R. Herczfeld, "The GaAs MESFET as an optically activated switch," in *High-Power Optically Activated Solid-State Switches*, A. Rosen and F. Zutavern, Eds. Norwood, MA: Artech House, 1993, ch. 9.

[9] S. M. Sze, *Physics of Semiconductor Devices*. New York: Wiley, 1981.

Tamera A. Yost received the Associate degree in electronic technology from Lincoln Technical Institute, Allentown, PA, in 1984, the B.S. degree in electrical and computer engineering from the State University of New York at New Paltz, in 1992, and the M.S. and Ph.D. degrees in electrical and computer from Drexel University, Philadelphia, PA, in 1994 and 1998, respectively.

From 1984 to 1992, she was with IBM, East Fishkill, NY, as a Senior Associate Engineer responsible for the design verification of semiconductor memory devices to be used in future IBM computer systems. Her research experiences cover topics such as optically controlled phased-array-antenna subsystem design at the Naval Air Warfare Center (NAWC), a cooperative effort with the Sarnoff Corporation in the analysis of a hybrid transversal filter for RADAR applications, substrate characterization in the millimeter range at the Army Research Laboratory (ARL), and work on a hybrid LIDAR-RADAR system for the NAWC. From 1998 to 2000, she was the Director of Research and Development at F&H Applied Science Associates Inc., Mt. Laurel, NJ. She is currently a Member of Technical Staff of the Electronic Product Division, W.L. Gore and Associates Inc., Newark, DE.

Dr. Yost is a member of the Society of Women Engineers and the Optical Society of America. She was the recipient of the Graduate Engineering Education Doctoral Fellowship for Women and Minorities in Education sponsored by the National Science Foundation (1992–1998).

Asher Madjar (M'73–SM'83–F'97) received the B.Sc. and M.Sc. degrees from the Technion, Israel Institute of Technology, Haifa, Israel, in 1967 and 1969, respectively, and the D.Sc. degree from Washington University, St. Louis, MO, in 1979.

Since 1969, he has been with RAFAEL, Haifa, Israel, and with the Technion. With RAFAEL, he has performed research in the areas of passive and active microwave devices. He headed the Microwave Integrated Circuit (MIC) Group from 1973 to 1976, served as a Microwave Chief Engineer in the Communications Department from 1979 to 1982, and as Chief Scientist of the Microwave Department from 1982 to 1989 with direct responsibility of the MMIC Group from 1987 to 1989. He is currently a Research Fellow involved in microwave optoelectronics activity, MMIC, monolithic circuits combining microwave and optical devices, and microwave modules. In the Technion and Ort Braude College, he teaches several courses on microwaves, passive microwave devices, active microwave devices, transmission and reception techniques, etc., and serves as an instructor for graduate students. From 1989 to 1991, he was a Visiting Professor at Drexel University, Philadelphia, PA. During that time, he performed research on optical control of microwave devices, and developed a comprehensive model for the optical response of the MESFET. He also participated in graduate student instruction and taught a course on microwave devices. He has authored or co-authored over 100 papers in the areas of microwave components and devices, MIC, MMIC, linear and nonlinear microwave circuits (harmonic balance, APFT, etc.), microwave device modeling (including optical effects), optical links at microwave frequencies, and more. He is on the Review Board of *Microwave Journal*

Dr. Madjar served as the Israel IEEE Antennas and Propagation Society (IEEE AP-S)/Microwave Theory and Techniques Society (IEEE MTT-S) chapter chairman for several years and, in that capacity, organized 13 symposia. From 1985 to 1989, he served as the secretary of the Israel Section of the IEEE. He also served on the Technical Committees for MELECON (1981), 14th 15th, 16th, 18th, and 19th conventions of Electrical and Electronics Engineers in Israel. Since 1990, he has served as a member of the Management Committee of the European Microwave Conference and, since 1993, as a member of the Technical Program Committee for the European Microwave Conferences. He also served as the Chairman of the 27th European Microwave Conference, Jerusalem, Israel, in 1997. In April 1996, he was elected to the newly created Steering Committee of the European Microwave Conference. He is a member of the Technical Program Committee of the 2001 International Microwave Symposium. He is on the Review Board of the IEEE TRANSACTIONS ON MICROWAVE THEORY AND TECHNIQUES, IEEE MICROWAVE AND GUIDED WAVE LETTERS. He was the recipient of the 1998 RAFAEL Best Researcher Prize .

Peter R. Herczfeld (S'66–M'67–SM'89–F'91) was born in Budapest, Hungary, in 1936. He received the B.S. degree in physics from Colorado State University, Fort Collins, in 1961, and the M.S. degree in physics and Ph.D. degree in electrical engineering from the University of Minnesota at Minneapolis. Paul, in 1963 and 1967, respectively.

Since 1967, he has been on the faculty of Drexel University, Philadelphia, PA, where he is currently the Lester Kraus Professor of Electrical and Computer Engineering. He is the Director of the Center for Microwave-Lightwave Engineering, Drexel University, a Center of Excellence that conducts research in microwaves and photonics. He has served as Project Director for more than 90 projects. He has authored or co-authored more than 400 papers in solid-state electronics, microwaves, photonics, solar energy, and biomedical engineering. He has advised 28 doctoral students and more than 70 masters students over his career. He has also served as a consultant to numerous large and small corporations (e.g., GE, 3M, AEL), Government laboratories (e.g., ARO, NRL, CECOM, NAWC), and educational institutions (e.g., University of Minnesota, BCC).

Dr. Herczfeld is a member of the IEEE Antennas and Propagation Society (IEEE APS-S). He is a recipient of several research and publication awards, including the European Microwave Prize (1986 and 1994). He is a recipient of the IEEE Millennium Medal and served as the Distinguished Lecturer of the IEEE Microwave Theory and Techniques Society (IEEE MTT-S). He initiated the Microwave Photonics Conferences, an IEEE Lasers and Electro-Optics Society (LEOS)–MTT joint venture, which has blossomed into a highly respected international meeting. He has received numerous teaching honors, including the Mary and Christian Lindback Distinguished Teacher Award from Drexel University and the IEEE MTT-S Fred Rosenbaum Distinguished Educator Award.